14th International Conference on Structural Safety and Reliability - ICOSSAR'25
1-6 June, 2025 - Los Angeles California, USA
R. Ghanem, E. Johnson, S. Masri and A. Olivier (Eds)

GENERATION OF STATIONARY WIND LOADS USING A STOCHASTIC WAVE-BASED APPROACH AND CFD SIMULATION FOR DYNAMIC ANALYSIS OF SOLAR PANEL ARRAYS

Hanshu Zhang[1*], You-Jia Li[2] and Matthew J. DeJong[3]

[1] University of California, Berkeley
508 Davis Hall, Berkeley, CA 94720
hzzhang@berkeley.edu

[2] University of California, Berkeley
516 Davis Hall, Berkeley, CA 94720
you-jia_li@berkeley.edu

[3] University of California, Berkeley
777 Davis Hall, Berkeley, CA 94720
dejong@berkeley.edu

Key words: Stochastic wind loads, Solar panel array modeling, Dynamic torsional strains

Abstract. This paper presents a novel simulation framework for estimating the dynamic response of a ground-mounted solar panel array under stationary wind loads which are spatially correlated across the length of the solar panel array. Specifically, the framework uses mean pressure coefficient distributions derived using the computational fluid dynamics (CFD) simulation software WE-UQ. Note that for the CFD simulation, the input wind field across the length of the solar panel array was uniform. The accuracy of the CFD simulation is validated by comparing the simulated mean pressure coefficients with those derived from wind tunnel tests. Next, simulated stochastic wind loads are generated from the stationary wind speed using a stochastic wave approach from the spectral representation method (SRM), as well as the mean pressure coefficients derived from the CFD simulation. Further, the simulated wind loads are applied to a solar panel array finite element model using the finite element software OpenSees to simulate dynamic response. Torsional strains on the torque tube are estimated to observe the performance of the solar panel array. The torsional strains obtained from the proposed wind generation method are compared with simulation results that use wind tunnel test data to define the loading; the proposed method generates significantly larger dynamic excitations, especially in higher vibration modes. This is primarily attributed to the spatially varying, but correlated, wind speeds. Consequently, the proposed simulation framework provides a valuable novel tool for solar panel array analysis.

1 INTRODUCTION

Solar energy generation has increased rapidly in recent years, which has motivated design optimization to minimize material use. However, as a result, ground-mounted solar panel arrays are vulnerable to damage under wind loads due to their shape, flexibility, and light-weight structure [1].

In this context, simulating the dynamic response of solar panel arrays is important for both design and analysis, particularly for extreme wind events. One option is physical simulation, for which wind tunnel testing has proven to be an effective and useful method. Miller and Zimmerman [2] conducted wind tunnel experiments to investigate the net mean pressure distributions on ground-mounted solar panel modules across various module tilt angles and wind directions. Aly and Bitsuamlak [3] applied wind tunnel tests to check how geometric scale of ground-mounted solar panel arrays affected pressure coefficients; it was concluded that peak wind loads are sensitive to geometric scales, instead mean wind loads are not significantly affected. Furthermore, [4] discussed details about computing wind pressures from wind tunnel tests. Abiola-Ogedengbe et al. [5] investigated wind effects on both upper and lower surfaces of solar modules using wind tunnel tests, with various wind directions and module elevation angles.

Although wind tunnel tests have proven useful, the experimental resources and time are substantial. As an alternative, computational fluid Dynamics (CFD) simulations are widely employed to analyze the wind effects on solar panel arrays. Shademan and Hangan [6] carried out CFD simulations to estimate the wind loads for various wind directions on ground-mounted solar panel arrays, and Bitsuamlak et al. [7] evaluated wind loads for numerous solar panel modules and wind directions using CFD. Further, Shademan et al. [8] assessed the effect of different flow configurations on wind loads and compared the simulated wind loads to experimental wind loads from wind tunnel tests. Shademan et al. [9] also carried out detached eddy simulation (DES) to analyze the influence of ground clearance on wind loads. Aly [10, 11] validated the effect of geometric scales on ground-mounted solar panel arrays by using CFD, and validated the CFD by comparing the results to wind tunnel tests.

These previous studies primarily focus on computing stationary wind loads from constant mean wind speed input and stationary pressure coefficient time histories obtained from wind tunnel tests or CFD. However, both methods still require substantial experimental and computational resources, respectively. Further, these methods do not account for the spatial variation of wind speeds that can occur across the full-scale horizontal length of large solar panel arrays. In this paper, a novel method to derive more realistic wind loads for dynamic simulation of full-scale ground-mounted solar panel arrays is proposed. Specifically, the wind velocities on solar panel arrays are simulated as a stationary stochastic wind field varying along one direction using the stochastic wave-based spectral representation method (SRM) [12, 13, 14, 15]. Next, only mean pressure coefficient distributions, obtained from CFD simulation, are required as input. The goal of the method is to provide a more efficient way to compute stationary stochastic wind loads on solar panel arrays, that are also more realistic compared to existing techniques. Using OpenSees, an example solar panel geometry is modeled, and its dynamic response under stationary stochastic wind loads is simulated. To evaluate the method, results from the proposed method are compared to results that directly employ experimentally measured stationary wind pressure time histories from wind tunnel tests as input.

2 Stationary stochastic wind load simulation

2.1 Constant wind velocities and pressure coefficient time histories (Case I)

In wind tunnel tests, pressures are usually measured at each pressure tap on a prototype scale model of a solar panel array. Fig. 1 shows an example wind tunnel test pressure tap layout, and also defines the wind azimuth direction and tilt angle. At each pressure tap, the time history of the pressure coefficient $C_p(t)$ can be obtained as Eq. (1) [5, 16, 17, 18]:

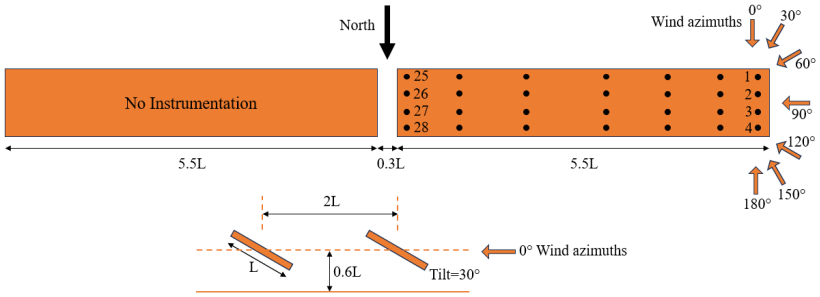

Figure 1: Example layout of a wind tunnel tests with points indicating pressure taps (geometry taken from [19]).

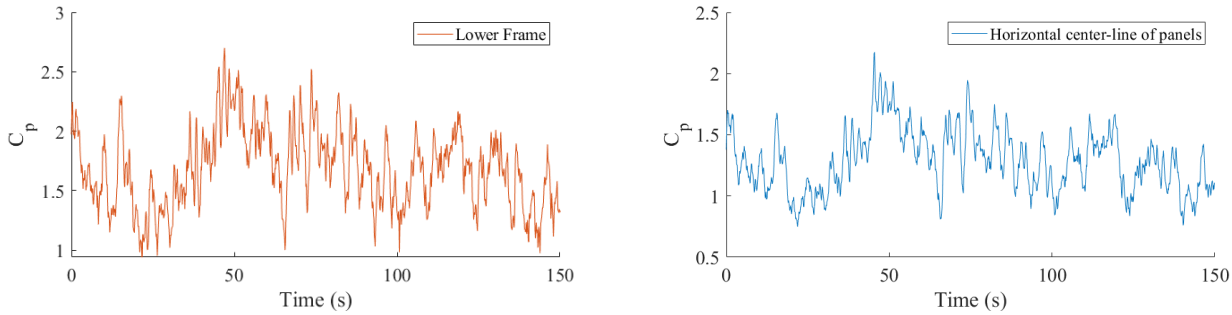

(a) (b)

Figure 2: Samples of pressure coefficient time histories.

$$C_p(t) = \frac{p(t) - p_\infty}{0.5\rho V_\infty^2}, \tag{1}$$

where $p(t)$ is the instantaneous pressure at the pressure tap, p_∞ is the atmospheric pressure, which is zero because the solar panel arrays are located in open terrain. ρ is the air density, and V_∞ is the mean wind velocity.

In this study, pressure coefficient time history distributions from [19] is used, with a wind azimuth direction of $0°$, a tilt angle of $-30°$, and a mean wind velocity of 9 m/s. Sample time histories of pressure coefficients from [19] are shown in Fig. 2. The locations of these pressure ports are highlighted with black dots in Fig. 1.

2.2 Stationary stochastic wind velocities and mean pressure coefficient distributions (Case II)

2.2.1 Stationary stochastic wind velocities

As noted above, Case II overcomes the limitation of the spatially constant wind speed simulated in wind tunnel tests. Specifically, instead of employing mean wind velocities in Eq. (1), stochastic wind velocities that vary in one spatial dimension are modeled as a stochastic wave that is continuous in both space and time [12, 15] as follows. The frequency-wavenumber spectrum can be expressed as

$$S(\omega, \kappa) = \frac{1}{2\pi} \int_{-\infty}^{\infty} S(\omega) \cdot \gamma(\xi, \omega) e^{i\kappa\xi} d\xi, \tag{2}$$

where $S(\omega, \xi)$ is the power spectrum, $\gamma(\xi, \omega)$ is the coherence function, ω is the frequency, ξ is the spatial distance, and κ is the wavenumber. This paper employs the Kaimal two-sided spectrum for wind velocity simulation and Davenport coherence function for spatial correlation [12, 15], the Eq. (2) can be expressed as

$$S(\omega,\kappa) = \frac{1}{2}\cdot\frac{200}{2\pi}\cdot u_*^2\cdot\frac{z}{U(z)}\cdot\frac{1}{\left[1+50\frac{\omega z}{2\pi U(z)}\right]^{\frac{5}{3}}}\quad\cdot\left[\frac{\frac{\lambda\omega}{\pi U(z)}}{\kappa^2+\left(\frac{\lambda\omega}{2\pi U(z)}\right)^2}\right], \tag{3}$$

where λ is a decay parameter [12, 15]. In this paper, $\lambda = 10$ is chosen for calculation. Then, z is the height above the ground, $U(z)$ is the average wind velocity at height z, and u_* is the velocity friction component defined as

$$u_* = \frac{kU(z)}{\ln(\frac{z}{z_0})}. \tag{4}$$

In Eq. (4), k represents von Karman's constant and $k = 0.4$ in this case, z_0 represents ground roughness, specified as 0.01 m since the solar panel array MI RTC is open terrain.

The Spectral Representation Method (SRM) can then be used to simulate sample realizations of a stochastic wave from its frequency-wavenumber spectrum [12, 13, 14, 15]. By mathematical manipulation, the sample realizations can be expressed in Fast Fourier Transform (FFT) and inverse Fast Fourier Transform (IFFT), shown as:

$$u(x,t) = \text{Re}\left[\text{FFT}_\kappa\left(\text{FFT}_\omega(B^{(1)})\right) + \text{FFT}_\kappa\left(\text{IFFT}_\omega(B^{(2)})\right)\right]. \tag{5}$$

with

$$B_{lm}^{(n)} = 2\sqrt{S(\omega_m,\kappa_l)\cdot\Delta\omega\Delta\kappa}\, e^{i\phi_{lm}^{(n)}}. \tag{6}$$

Further, the total stationary wind speed can be derived with constant mean wind speed and wind turbulence, shown as

$$\tilde{u}(x,t) = U(z) + u(x,t). \tag{7}$$

In this section, the constant mean wind speed at the reference height of the solar panel array is assumed to be 9 m/s at the height of horizontal center-line of solar panels, and the wind velocity profile follows the wind power law, as it was in Section 2.1. Sample realizations of wind velocities in both space and time are shown in Fig. 3. Further, the accuracy of the simulated wind velocity can be validated by comparing the power spectrum of the simulated wind velocity to the Kaimal spectrum. The power spectrum of the simulated $u(x,t)$ can be estimated from [12]

$$S_{jj}(\omega) = \frac{|\int_0^T u(x_j,t)e^{-i\omega t}dt|^2}{2\pi T}, \tag{8}$$

where $u(x_j,t)$ denotes the simulated wind velocities at location $x_j = 2$ m, and T denotes the duration of time. Fig. 4 shows that the estimated power spectrum from Eq. (8) matches the Kaimal spectrum [20]. Additionally, the accuracy of the simulated wind can be validated by comparing the estimated and target cross spectra. For sample realizations $u(x_j,t)$ and $u(x_k,t)$, cross spectra can be obtained from

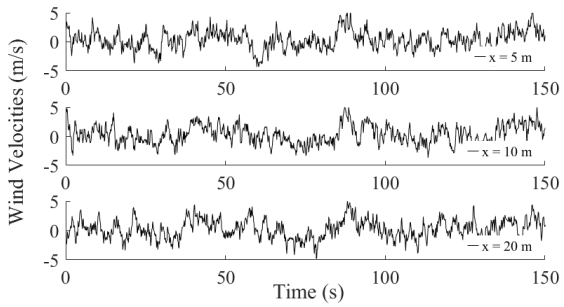

(a) Fluctuating component of wind velocity, $u(x,t)$

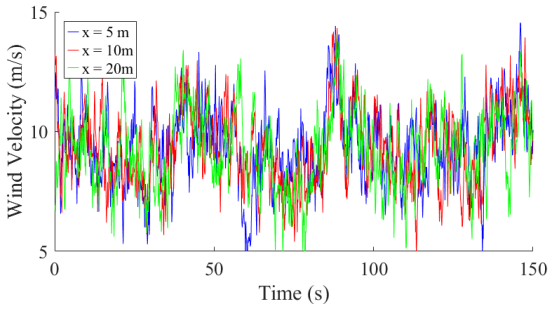

(b) Total stationary wind velocities, $u(x,t)$

Figure 3: Sample realization of stationary wind velocities in space and time.

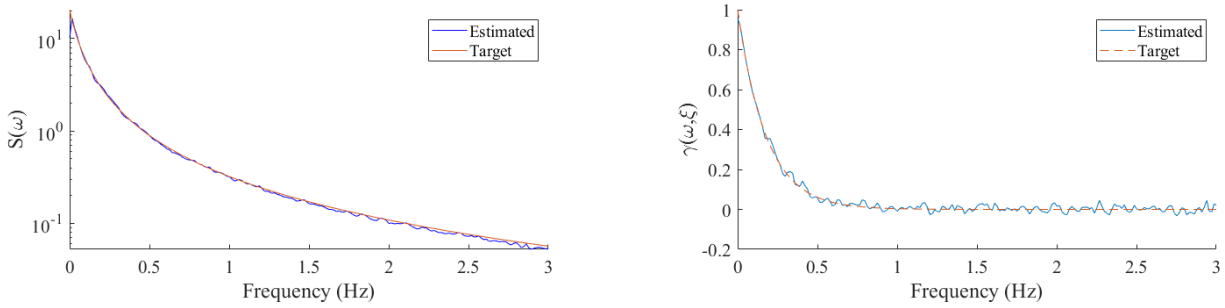

(a) (b)

Figure 4: Example comparison of the estimated and target: (a) power spectrum and (b) coherence function.

$$S_{jk}(\omega) = \frac{\int_0^T u(x_j,t)e^{-i\omega t}dt \int_0^T u(x_k,t)e^{-i\omega t}dt}{2\pi T}, \tag{9}$$

and the coherence functions are estimated as

$$\gamma(\xi_{jk},\omega) = \frac{S_{jk}(\omega)}{S_{jj}(\omega)S_{kk}(\omega)}. \tag{10}$$

In this section, three locations ($x_1 = 5$ m, $x_2 = 10$ m, and $x_3 = 20$ m) are used to assess the estimated cross spectra. Therefore, the separation distances are $\xi_{12} = 5$ m, $\xi_{13} = 15$ m, $\xi_{23} = 10$ m. Estimated coherence functions in Eq. (10) and Davenport coherence functions are shown in Fig. 4. Satisfactory agreement is achieved between the estimated and target coherence functions.

2.2.2 Mean pressure coefficient distributions

In general, the mean pressure coefficient distributions on solar panel arrays can be obtained from wind tunnel tests. However, the measurement of mean pressure coefficient distributions still requires physical experiments. In this regard, the CFD simulation procedure from WE-UQ [21, 22] is applied to estimate the mean pressure coefficient distributions, and the results are validated by comparing them to the mean pressure coefficient distributions from wind tunnel tests in section 2.1. In WE-UQ, the basic geometries of a 1:10 scale of the solar panel model at MI RTC can be modeled and imported, as shown in Fig. 5. Then, WE-UQ can establish the mesh and boundaries based on the

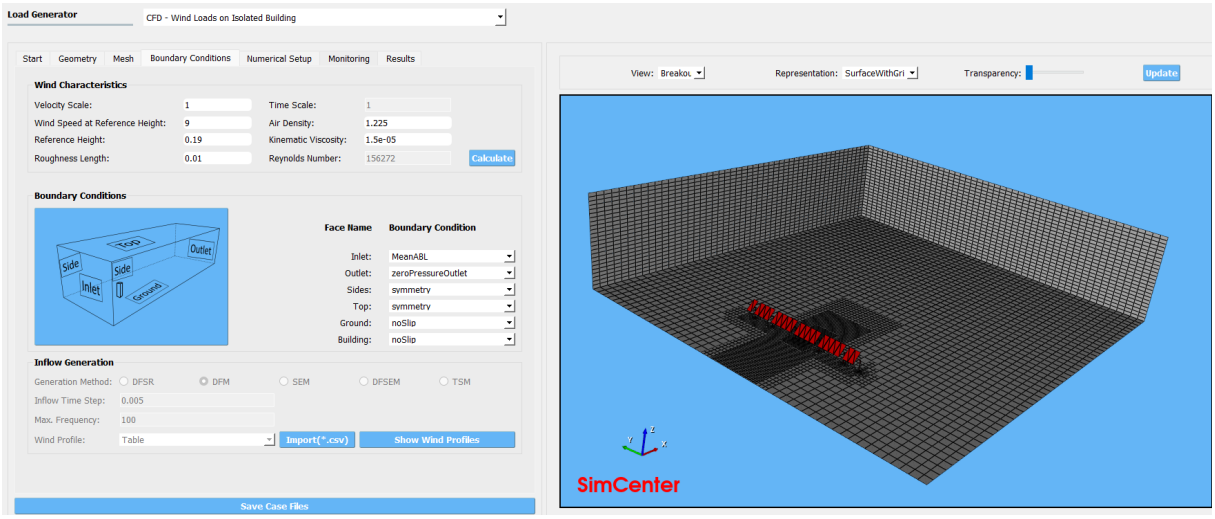

Figure 5: Screenshot of the WE-UQ app user interface.

imported model. The boundary conditions shown in Fig. 5 are configured to replicate the environmental conditions observed at the MI RTC solar panel array site, ensuring consistency between the CFD simulation and the actual testing environment. The ground roughness is 0.01 to make sure the value is consistent with the value in Section 2.2.1. Then, the values of air density and kinematic viscosity of the air assumed by WE-UQ [21, 22] and shown in Fig. 5 can be used for simulation. Next, the constant mean wind speed is 9 m/s, and the wind profile input, imported to estimate the pressure coefficients, is identical to the constant mean wind speed values from wind tunnel tests in Section 2.1 and wind profile in Section 2.2.1. In this regard, it is proposed that the mean pressure coefficients from only the constant smooth flow wind needs to be obtained. There are two reasons to propose this novel idea. First, the mean pressure coefficient distributions are normally obtained from constant mean wind speed and fluctuating turbulence, which takes substantial computational resources and time. This idea can significantly reduce the computational resources and time to run CFD simulation. Second, it is observed that over a sufficiently long time period, the mean pressure coefficient distributions under stationary smooth and turbulent wind inflows are hypothesized to exhibit similar patterns.

To assess the precision of CFD simulation, the mean pressure coefficients by CFD and ratio of mean pressure coefficient distributions between CFD simulation from stationary smooth flow wind and wind tunnel tests from stationary turbulence inflow (shown in Fig. 1) are shown in Fig. 6. As it can be seen, mean pressure coefficients are generally larger when the height of the modules decrease, and the ratio distributions are close to 1.0 in most locations, which validates the proposed method to obtain mean pressure coefficients from constant smooth flow wind. However, at two very local positions, the ratio is larger than 1.5, which means the pressure coefficients recorded from wind tunnel tests are much more smaller. The large and seemingly anomolously low pressure at these locations could be due to pressure tap measurement errors, and thus may not accurately reflect the wind effects at these locations.

Additionally, as mentioned in Section 1, peak pressure coefficients are significantly influenced by the geometric scale of the solar panel array, while mean pressure coefficients are not significantly influenced by model size. Thus, the use of mean pressure coefficients rather than time histories reduces potential scaling errors.

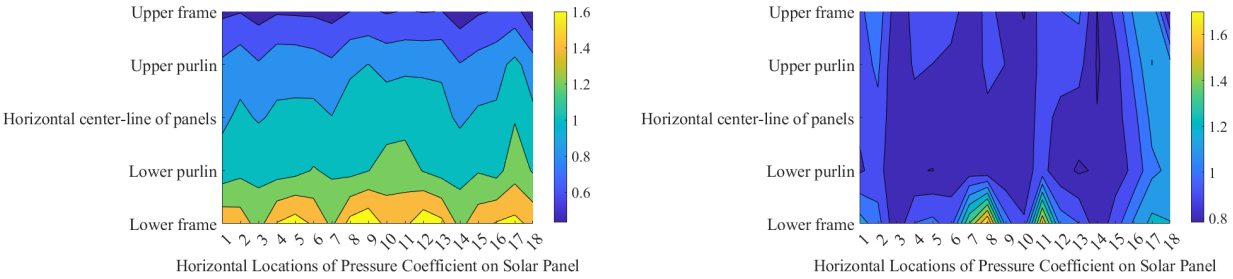

Figure 6: Mean pressure coefficient distributions on the solar panel model: (a) by CFD simulation, and (b) ratio between CFD simulation and wind tunnel tests.

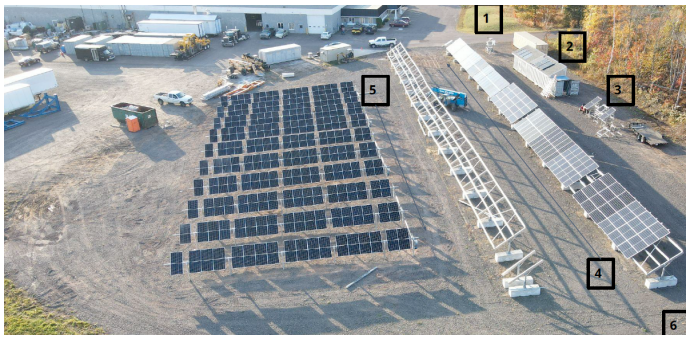

Figure 7: MI Solar Regional Test Center (MI RTC) in Michigan.

Furthermore, the dynamic wind pressure can be computed as

$$p(x,t) = 0.5\rho u(x,t)\bar{C}_p + \rho_\infty, \tag{11}$$

where $u(x,t)$ is again the simulated stationary stochastic wind velocity and $\bar{C}_p$ is the mean pressure coefficient, both are distributed on a solar panel array model. Wind loads and dynamic response of solar panel arrays will be simulated to assess whether the proposed method provides sufficient accuracy and improved computational efficiency.

3 Dynamic analysis of a solar panel array

To demonstrate and evaluate the proposed method to generate stochastic wind loads, the geometry of the solar panel array located at the Michigan Solar Regional Test Center (MI RTC), shown in Fig. 7, was used to create a simulation model. This site has 10 rows of solar panel arrays, each with a length of 22.2 m and a height of 1.83 m. The spacing between adjacent arrays is 5.18 m. Each array has 18 panels, each of which is 2.024 m by 1.002 m in size. On each row, a compression spring and a hydraulic damper are attached to the left end of the torque tube of the solar panel array in Fig. 7, while the right end of the torque tube is fixed to the tracker motor, and assumed unable to rotate in the simulations below.

Further, a finite element (FE) model of a single-axis solar panel array was built in OpenSees, as shown in Fig. 8 [20]. Fig. 8 also identifies specific locations that will be used to present and analyze the results in this paper. Specifically, torsional time histories on the torque tube (T1-T3) are obtained to interpret the displacements of the entire solar panel array, and are used to compute torsional strains on green color lines highlighted in Fig. 8. Further, the model primarily consists of beam-column

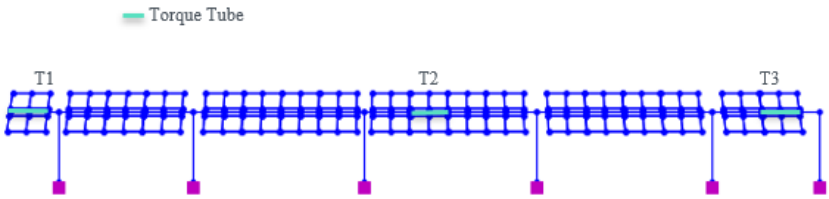

Figure 8: A solar panel array model by OpenSees. T1 - T3 are locations used for presenting results.

elements used to represent the structural components shown in Table 1. The Young's modulus for steel and glass are specified as 200 GPa and 68.3 GPa, respectively [20]. Meanwhile, the panels themselves were modeled as 'Elastic Membrane Plate' elements [20]. To account for the damping and stiffness of the solar panel array, as well as the hydraulic damper, a modal damping ratio of 0.09 was specified for the first four modes and stiffness proportional damping, with a stiffness proportional coefficient of 0.0103, was used to damp higher modes [20]. The hydraulic damper attached to the solar panel array contributes to the relatively high damping and improved structural safety. Furthermore, the dynamic characteristics of the FE model are evaluated by identifying the modes that may be relevant for interpreting wind loading response. The first four natural frequencies are $2.75, 3.38, 4.07$, and 4.9 Hz, respectively [20]. Some mode shape plots are shown in Fig. 9. The mode shapes look as expected, with bending of the columns and torsion of the torque tube dominating the first four mode shapes. For higher modes, such as Mode 10 (6.065 Hz), more localized deformations dominate, exemplified by local bending at the end of the torque tube in Mode 10 [20].

Table 1: OpenSees model properties

	Discription	**Size**
Torque Tube	Octagon main axis that runs through the array and supports the panels.	Side Length: 1.75" Thickness: 1/4" Total Length: 21.3"
Support Column	A total of six columns, each with a height of 1.83m.	Depth: 6" Flange Thickness: 0.25" Flange Width: 4" Web Thickness: 3/8"
Module	Modeled with shell elements with glass material properties - ShellMITC4 in OpenSees.	Thickness: 0.16" Panel Length: 79.69" Panel Width: 39.45
Frame	Rectangular tubes that hold the modules in place.	Cross Section: 1.18" $\times$ 0.47" (including Hollow Section: 0.925" $\times$ 0.44")
Purlin/Connector	Purlins are the connection between the torque tube and the frame. Purlins are C-shape.	Length: 12"

4 Results and discussions

Sample dynamic wind pressure time histories and power spectra of the lower frame edge of the solar panel array, produced using the two methods, are shown in Fig. 10. Note that the pressures from Case II are generally larger compared to the pressures from Case I. Again, the power spectra from Case II are more powerful than those obtained from Case I. Using the generated wind pressures from both cases, the structural response was simulated.

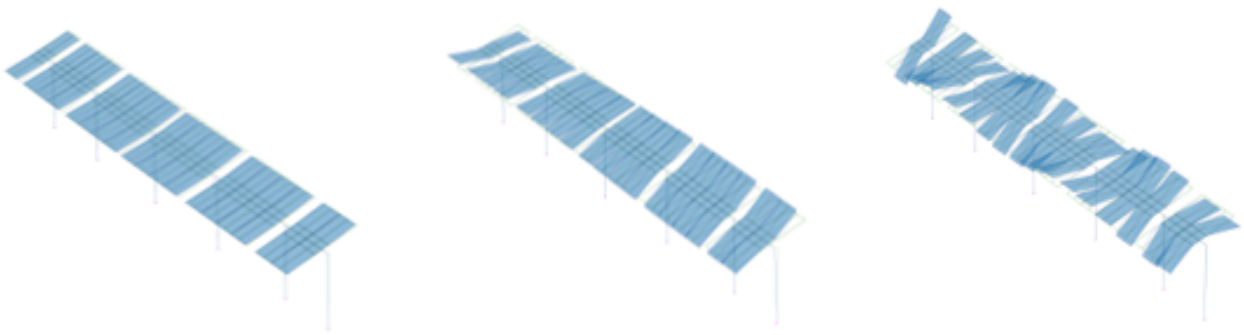

(a) Mode 2 (b) Mode 4 (c) Mode 10

Figure 9: Mode shapes of the solar panels array.

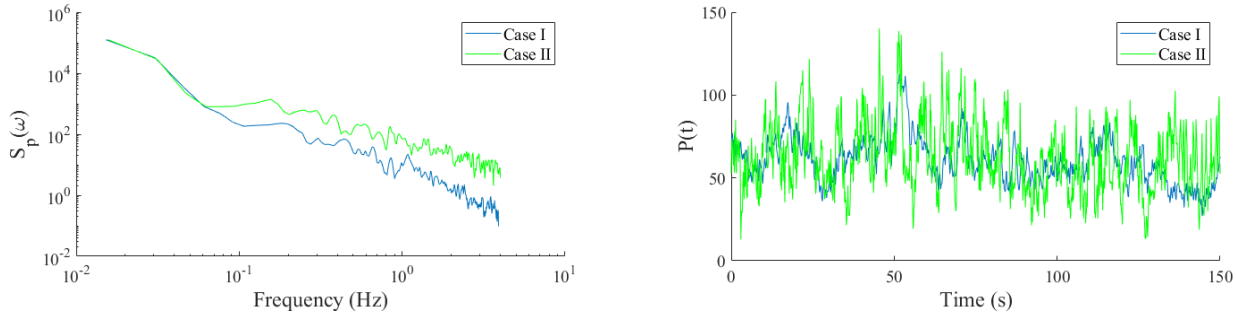

(a) (b)

Figure 10: Sample pressure time histories and power spectra for each of the proposed methods.

Further, the torque tube in the solar panel array is used to rotate the modules with respect to the position of the sun. So it must be designed to withstand the torque induced by twisting during heavy winds. Additionally, the distribution of twist along the torque tube gives an indication of the global response of the structure. Monitoring the torsional movement of the torque tube under wind loads is useful to ensure that the torque tube can prevent system failures and the dynamic response can be further understood.

The spectrograms of torsional strain at location T3 in Fig. 8, under the two different loading cases, are shown in Fig. 11. The solid and dashed-dot black lines represent the mean value of frequency and standard deviation of frequency, respectively. As it can be observed in Fig. 11, the spatially-correlated stochastic wind loads in Case II excite higher modes on the torque tube more than the wind loads generated using Case I.

Further, for engineering design, the peak strains of the torque tube are of interests. Time series of the torsional strains at locations T1, T2, and T3 in Fig. 8 are shown in Fig. 12 for both cases. Note that the right end of the solar panel array model is fixed to the motor, while the left end is assumed free to rotate, so the torsional strain value at the right end of the torque tube (T3) is the largest among the three locations. In Fig. 12, the torsional strains induced by Case I are much smaller, demonstrating that including the spatially varying wind generation method has a large effect on the peak strains predicted.

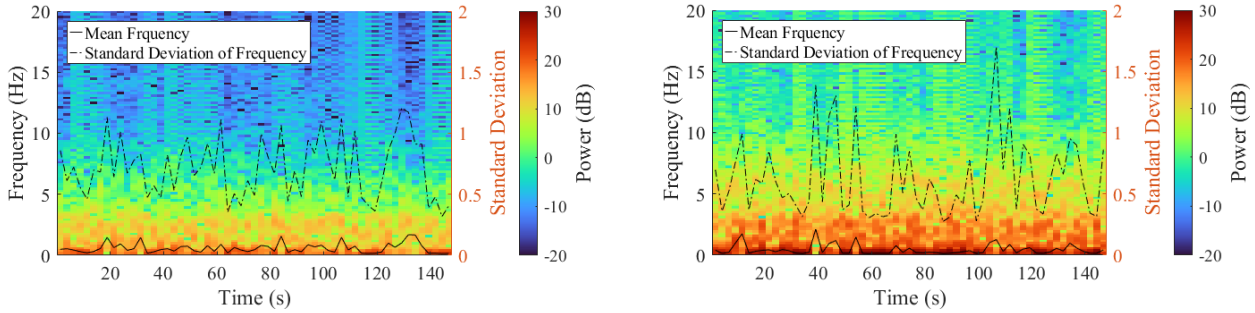

(a) Case I at T3

(b) Case II at T3

Figure 11: Spectrogram of the torsional strain (location T3 in Fig. 8).

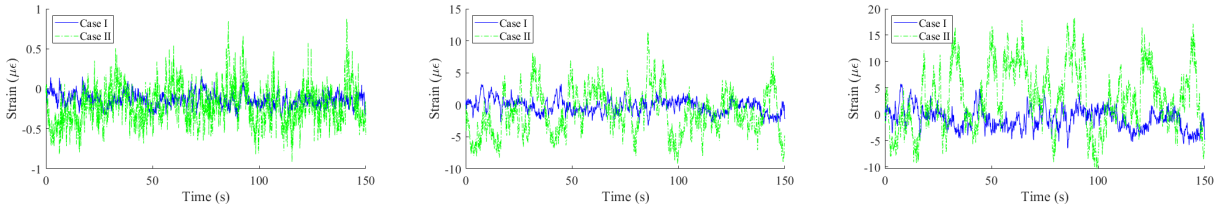

(a) T1

(b) T2

(c) T3

Figure 12: Torsional Strain at three locations.

5 Conclusions

In this paper, the problem of simulating the dynamic response of solar panel arrays under dynamic wind loads is addressed. For this purpose, stationary stochastic wind pressures are measured and computed from pressure taps installed on a prototype solar panel array in wind tunnel tests (Case I). Based on the measured data, a novel method for generating spatially varying stationary stochastic wind pressure time histories (Case II) that can be applied at each location across the entire face of full-scale panel array, was proposed. Finite element modeling was then used to simulate the dynamic response of an example array at MI RTC. The effect of the wind generation method on the dynamic response of the panel array was then explored.

The new method (Case II) results in larger torsional strains than Case I. In particular, Case II causes a much larger excitation of higher modes, which are shown to be dominant in the magnitude of torsional strain experienced by the torque tube. Further, Case II requires significantly less computation time than Case I. Thus, Case II may provide designers and analysts with a useful, computationally efficient method of generating spatially correlated stationary wind pressure time histories across the length of solar panel arrays, and therefore more accurately capture the excitation of higher modes that might be important in torque tube design.

Acknowledgements

The authors gratefully acknowledge the financial support from the U.S. Department of Energy (DOE) Solar Energy Technology Office (SETO) (project DE-FOA-0002597: Renewables Advancing Community Energy Resilience (RACER)). The authors also gratefully acknowledge the dataset provided by Dr. Xinlong Du and Dr. Tracy Becker from the University of California, Berkeley, and the guidance of WE-UQ application by Dr. Abiy Melaku from the SimCenter at the University of

California, Berkeley.

REFERENCES

[1] M. Moravej, A. G. Chowdhury, P. Irwin, I. Zisis, and G. Bitsuamalk. Dynamic effects of wind loading on photovoltaic systems. In *14th International Conference on Wind Engineering (ICWE14)*, Porto Alegre, Brazil, 2015.

[2] R. D. Miller and D. K. Zimmerman. Wind loads on flat plate photovoltaic array fields. phase iii, final report. Technical Report NREL/TP-5500-67456, Boeing Engineering and Construction Co., Seattle, WA, USA, 1981.

[3] A. M. Aly and G. Bitsuamlak. Aerodynamics of ground-mounted solar panels: Test model scale effects. *Journal of Wind Engineering and Industrial Aerodynamics*, 123:250–260, 2013.

[4] A. Schellenberg, J. Maffei, K. Telleen, and R. Ward. Structural analysis and application of wind loads to solar arrays. *Journal of Wind Engineering and Industrial Aerodynamics*, 123:261–272, 2013.

[5] A. Abiola-Ogedengbe, H. Hangan, and K. Siddiqui. Experimental investigation of wind effects on a standalone photovoltaic (pv) module. *Renewable Energy*, 78:657–665, 2015.

[6] M. Shademan and H. Hangan. Wind loading on solar panels at different inclination angles. In *11th Americas conference on wind engineering*, San Juan, Puerto Rico, 2009.

[7] G. T. Bitsuamlak, A. K. Dagnew, and J. Erwin. Evaluation of wind loads on solar panel modules using cfd. In *Proceedings of the fifth international symposium on computational wind engineering*, Chapel Hill, NC, USA, 2010.

[8] M. Shademan, R. M. Barron, R. Balachandar, and H. Hangan. Numerical simulation of wind loading on ground-mounted solar panels at different flow configurations. *Canadian Journal of Civil Engineering*, 41(8):728–738, 2014.

[9] M. Shademan, R. Balachandar, and R. M. Barron. Detached eddy simulation of flow past an isolated inclined solar panel. *Journal of fluids and structures*, 50:217–230, 2014.

[10] A. M. Aly and G. Bitsuamlak. Aerodynamic loads on ground-mounted solar panels: multi scale computational and experimental investigations. In *Advances in Civil, Environmental, and Materials Research (ACEM14)*, 2014.

[11] A. M. Aly. On the evaluation of wind loads on solar panels: The scale issue. *Solar Energy*, 135:423–434, 2016.

[12] B. A. Benowitz and G. Deodatis. Simulation of wind velocities on long span structures: A novel stochastic wave based model. *Journal of Wind Engineering and Industrial Aerodynamics*, 147:154–163, 2015.

[13] L. Peng, G. Huang, A. Kareem, and Y. Li. An efficient space–time based simulation approach of wind velocity field with embedded conditional interpolation for unevenly spaced locations. *Probabilistic Engineering Mechanics*, 43:156–168, 2016.

[14] L. Peng, G. Huang, X. Chen, and A. Kareem. Simulation of multivariate nonstationary random processes: Hybrid stochastic wave and proper orthogonal decomposition approach. *Journal of Engineering Mechanics*, 143(9):04017064, 2017.

[15] J. Chen, Y. Song, Y. Peng, and P. D. Spanos. Simulation of homogeneous fluctuating wind field in two spatial dimensions via a joint wave number–frequency power spectrum. *Journal of Engineering Mechanics*, 144(11):04018100, 2018.

[16] C. W. Letchford, R. E. Iverson, and J. R. McDonald. The application of the quasi-steady theory to full scale measurements on the texas tech building. *Journal of Wind Engineering and Industrial Aerodynamics*, 48(1):111–132, 1993.

[17] J. D. Holmes. *Wind loading of structures*. CRC press, 2007.

[18] E. Simiu and D. H. Yeo. *Wind effects on structures: Modern structural design for wind*. John Wiley Sons, 2019.

[19] X. Du, T. Becker, Z. Taylor, and C. Needham. Demands on solar structural joints under wind loading. *Journal of Structural Engineering*.

[20] H. Zhang, Y. Li, and M. J. DeJong. Simulation of dynamic response of solar panel arrays under stochastic wind loads. *Journal of Wind Engineering Industrial Aerodynamics*.

[21] F. McKenna, A. Melaku, P. Mackenzie-Helnwein F. Ding, M. Gardner, S. Yi, A. B. Satish, and W. Elhaddad. Nheri-simcenter/we-uq: Version 4.2.0, 2025.

[22] G. G. Deierlein, F. McKenna, A. Zsarnóczay, T. Kijewski-Correa, A. Kareem, W. Elhaddad, Laura Lowes, Matthew J. Schoettler, and S. Govindjee. A cloud-enabled application framework for simulating regional-scale impacts of natural hazards on the built environment. *Frontiers in Built Environment*, 6:558706, 2020.